Critical suppression of spin Seebeck effect by magnetic fields

Takashi Kikkawa,[1,2] Ken-ichi Uchida,[1,3,*] Shunsuke Daimon,[1] Zhiyong Qiu,[2,4] Yuki Shiomi,[1,4] and Eiji Saitoh[1,2,4,5]

[1]*Institute for Materials Research, Tohoku University, Sendai 980-8577, Japan*
[2]*WPI Advanced Institute for Materials Research, Tohoku University, Sendai 980-8577, Japan*
[3]*PRESTO, Japan Science and Technology Agency, Saitama 332-0012, Japan*
[4]*Spin Quantum Rectification Project, ERATO, Japan Science and Technology Agency, Sendai 980-8577, Japan*
[5]*Advanced Science Research Center, Japan Atomic Energy Agency, Tokai 319-1195, Japan*

The longitudinal spin Seebeck effect (LSSE) in Pt/$Y_3Fe_5O_{12}$ (YIG) junction systems has been investigated at various magnetic fields and temperatures. We found that the LSSE voltage in a Pt/YIG-slab system is suppressed by applying high magnetic fields and this suppression is critically enhanced at low temperatures. The field-induced suppression of the LSSE in the Pt/YIG-slab system is too large at around room temperature to be explained simply by considering the effect of the Zeeman gap in magnon excitation. This result requires us to introduce a magnon-frequency-dependent mechanism into the scenario of LSSE; low-frequency magnons dominantly contribute to the LSSE. The magnetic field dependence of the LSSE voltage was observed to change by changing the thickness of YIG, suggesting that the thermospin conversion by the low-frequency magnons is suppressed in thin YIG films due to the long characteristic lengths of such magnons.

I. INTRODUCTION

Magnons are collective excitations of spins in magnetic ordered states, the concept of which was first introduced by Bloch in order to explain the temperature dependence of magnetization in a ferromagnet [1]. In thermal equilibrium states, magnons behave as weakly interacting bosonic quasiparticles obeying the Bose-Einstein distribution:

$$f_{BE}(\epsilon, T_m) = \frac{1}{\exp(\epsilon/k_B T_m) - 1}, \qquad (1)$$

where ϵ is the magnon energy, k_B is the Boltzmann constant, and T_m is the magnon temperature. In soft magnetic materials such as $Y_3Fe_5O_{12}$ (YIG) [2], magnons are easily excited by thermal energy since the magnon dispersion is almost gapless except for a small gap due to the Zeeman effect and magnetic anisotropy ($\sim 10^{-3}$ K for YIG [3,4]).

In the field of spintronics [5,6], magnons have attracted renewed attention, since they can carry a spin current without accompanying a charge current [7,8]. Importantly, a magnon spin current in a magnet can interact with a conduction-electron spin current in an attached metal at the metal/magnet interface via the interface exchange interaction, which is described in terms of the spin-mixing conductance [9–11]. By making use of this interaction, various spin-current-related phenomena have been developed, such as the spin pumping [8,12,13], spin Seebeck effect (SSE) [14–38], and their reciprocal effects [8,39].

The SSE refers to the generation of a spin current as a result of a temperature gradient in a magnetic material. Here, the thermally generated spin current is detected as electric voltage (SSE voltage) via the inverse spin Hall effect (ISHE) [12,13,40–42] in a paramagnetic metal attached to a magnet. The observation of the SSE in a ferrimagnetic insulator YIG [15,17] implies that this phenomenon is attributed to nonequilibrium magnon dynamics driven by a temperature gradient, since a conduction electrons' contribution in YIG is frozen out due to its large charge gap. After the pioneering theoretical work by Xiao *et al.* [43], the SSE is mainly described in terms of the effective magnon temperature T_m in a ferrimagnet and effective electron temperature T_e in an attached paramagnetic metal; when the effective magnon-electron temperature difference is induced by an external temperature gradient, a spin current is generated across the ferrimagnet/paramagnet interface. Adachi *et al.* developed linear-response theories of the magnon- and phonon-mediated SSEs [44–46]. Subsequently, Hoffman *et al.* formulated a Landau-Lifshitz-Gilbert theory of the SSE to investigate the thickness dependence and length scale of the SSE [47]. In 2014, Rezende *et al.* discussed the SSE in terms of a bulk magnon spin current created by a temperature gradient in a ferrimagnetic insulator [31]. However, microscopic understanding of the relation between the magnon excitation and thermally generated spin currents is yet to be established, and more systematic experimental studies are necessary.

A clue to understand a role of magnons in SSE already manifested itself in magnetic-field-dependence measurements. In Ref. [29], we showed that the magnitude of the SSE voltage in paramagnetic-metal (Pt, Au)/YIG-slab junction systems gradually decreases with increasing the magnetic field after taking its maximum value at room temperature [see Fig. 1(b)]. This suppression of the SSE voltage becomes apparent by applying high magnetic fields, while it is very small in the conventional SSE measurements in a low-field range [see Fig. 1(c)]. The SSE suppression by high magnetic fields is irrelevant to the anomalous Nernst effect due to static proximity ferromagnetism in Pt [48] since the same behavior was observed not only in Pt/YIG-slab systems but also in Au/YIG-slab systems [29] (note that Au is free from the proximity ferromagnetism). Although this result implies that the SSE is affected by a magnon gap opening due to the Zeeman effect, there was no detailed discussion on the high-magnetic-field behavior of the SSE. In this study,
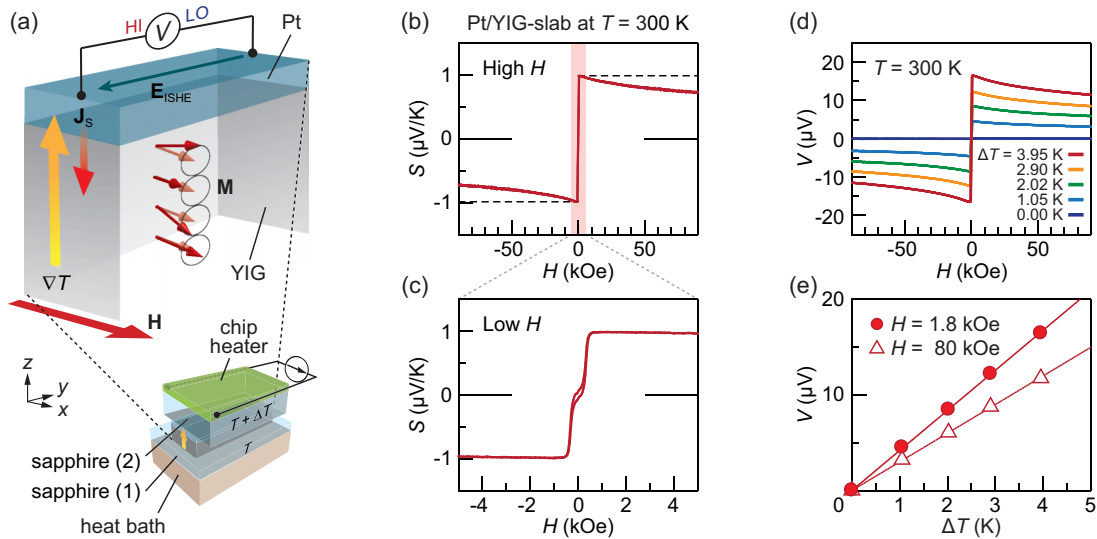
---

*kuchida@imr.tohoku.ac.jp

FIG. 1. (Color online) (a) A schematic illustration of the LSSE in the Pt/YIG sample and experimental setup used in the present study. The sample is sandwiched between two sapphire plates (1) and (2). The temperatures of the sapphires (1) and (2) were respectively stabilized at T and $T + \Delta T$, where ΔT (>0) is a temperature difference. ∇T, V, $\mathbf{H}$, $\mathbf{M}$, $\mathbf{E}_{\mathrm{ISHE}}$, and $\mathbf{J}_s$ denote the temperature gradient along the $+z$ direction, electric voltage between the ends of the Pt layer, magnetic field vector with the magnitude H, magnetization vector with the magnitude M, electric field induced by the ISHE, and spatial direction of the thermally generated spin current, respectively. (b), (c) H dependence of the transverse thermopower S in the Pt/YIG-slab sample at $T = 300$ K, measured when H was swept between ± 90 kOe (b) and ± 5 kOe (c). (d) H dependence of V in the Pt/YIG-slab sample at $T = 300$ K for various values of ΔT. (e) ΔT dependence of V in the Pt/YIG-slab sample at $T = 300$ K at $H = 1.8$ kOe (closed circles) and 80 kOe (open triangles).

using Pt/YIG systems, we systematically investigated effects of high magnetic fields on the SSE at various temperatures ranging from 300 K to 5 K. We also report the YIG-thickness dependence of the SSE voltage and its suppression at high magnetic fields. The results suggest an important role of excitation of low-frequency magnons with long characteristic lengths in the SSE, providing an important step in unraveling the nature of the SSE.

II. EXPERIMENTAL CONFIGURATION AND PROCEDURE

Experiments on the SSE have been performed mainly in a longitudinal configuration owing to its simplicity [17,20–38], and we also employ this configuration in this study. Figure 1(a) shows a schematic illustration of the longitudinal SSE (LSSE). In the longitudinal configuration, when a temperature gradient, ∇T, is applied to a paramagnetic-metal/ferrimagnetic-insulator junction system perpendicular to the interface, a spin current is thermally generated in the paramagnetic layer along the ∇T direction. The spin current is converted into an electric field $\mathbf{E}_{\mathrm{ISHE}}$ by the ISHE in the paramagnetic layer if the spin-orbit interaction of the paramagnet is strong [see Fig. 1(a)]. When the magnetization $\mathbf{M}$ of the ferrimagnet is along the x direction, $\mathbf{E}_{\mathrm{ISHE}}$ is generated in the paramagnet along the y direction following

$$\mathbf{E}_{\mathrm{ISHE}} = (\theta_{\mathrm{SH}}\rho)\mathbf{J}_s \times \boldsymbol{\sigma}, \qquad (2)$$

where θ_{SH}, ρ, $\mathbf{J}_s$, and $\boldsymbol{\sigma}$ are the spin Hall angle, electric resistivity, spatial direction of a spin current, and spin-polarization vector of electrons ($||\mathbf{M}$) in the paramagnet, respectively. Therefore, the LSSE can be detected electrically by measuring

electric voltage V_{ISHE} ($=E_{\mathrm{ISHE}}L_y$) in the paramagnetic metal layer, where E_{ISHE} is the magnitude of $\mathbf{E}_{\mathrm{ISHE}}$ and L_y is the length of the paramagnetic layer along the y direction.

To investigate the high-magnetic-field behavior of the LSSE, we used Pt/YIG junction systems, which are now recognized as a model system for studying spin-current physics [8,15]. The sample used in the present study consists of a 5-nm-thick Pt film sputtered on the whole of the (111) surface of a single-crystalline YIG slab or film. The Pt films were formed on all the YIG samples at the same time. The YIG slab has no substrate, of which the lengths along the x, y, and z directions are $L_x = 2.0$ mm, $L_y = 4.0$ mm, and $L_z = 1.0$ mm, respectively. To measure the thickness dependence of the LSSE, we prepared three YIG films with the thicknesses of $t_{\mathrm{YIG}} = 10.42\ \mu$m, $1.09\ \mu$m, and $0.31\ \mu$m, grown on the whole of single-crystalline $\mathrm{Gd_3Ga_5O_{12}}$ (GGG) (111) substrates by a liquid phase epitaxy method [11]. All the YIG films were prepared under the same growth condition. The GGG substrates with the YIG films were then cut into a rectangular shape with the size of $L_x = 2.0$ mm, $L_y = 4.0$ mm, and $L_z = 0.5$ mm. Before forming the Pt films, the surface of the YIG slab and films were mechanically polished with alumina powder with the diameter of $0.05\ \mu$m; the resultant surface roughness of the YIG slab and films are very small and comparable to each other as shown in the atomic force microscope images in Fig. 2.

In Fig. 3, we show the temperature T dependence of the magnetization M for the YIG slab at $H = 1.8$ kOe [Fig. 3(a)] and for the YIG films at $H = 0.3$ kOe [Figs. 3(b)–3(d)]. Here, the M values for the YIG films were obtained by subtracting the contributions from the paramagnetic GGG substrates. As T decreases, the M values monotonically increase and
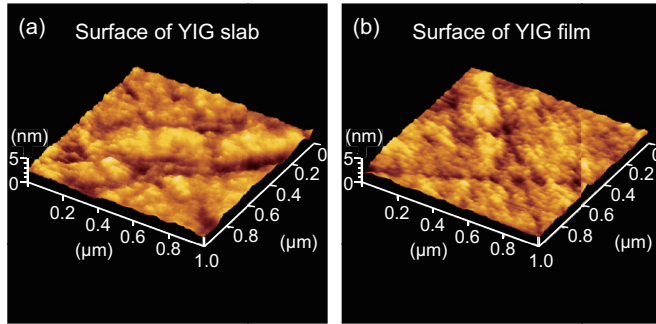
FIG. 2. (Color online) Atomic force microscope images of the surface of the YIG-slab (a) and YIG-film (b) samples, where the surface roughness R_a is less than 0.3 nm for both the samples. All the YIG-film samples with the different thicknesses were prepared under the same growth condition by means of a liquid phase epitaxy method. After the growth, their surfaces were mechanically polished under the same condition; all the YIG films have similar surface roughness.

approach $\sim 5\mu_B$, with μ_B being the Bohr magneton, at the lowest temperature in all the YIG samples, consistent with the literature value [49]. We found that the observed T dependence of M follows the Bloch law [1]:

$$M = M_0(1 - \zeta T^{3/2}), \qquad (3)$$

where M_0 is the saturation magnetization at $T = 0$ K and ζ is a constant. By fitting the experimental data with Eq. (3), we ob-

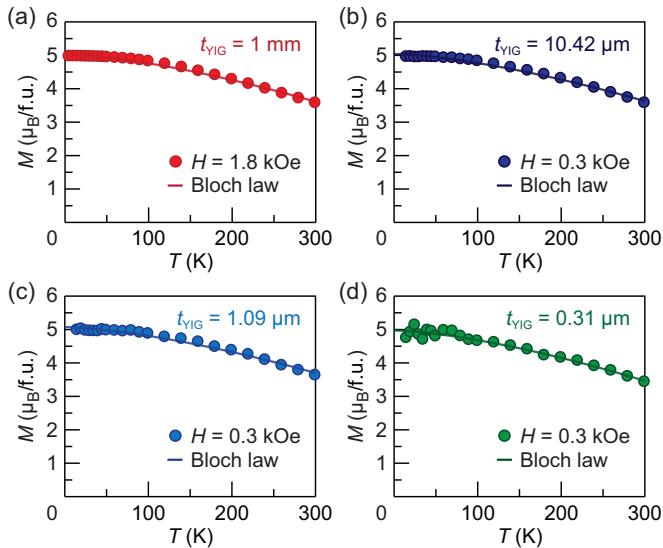FIG. 3. (Color online) T dependence of M for the YIG-slab sample with $t_{YIG} = 1$ mm (a) at $H = 1.8$ kOe and in the YIG-film samples with $t_{YIG} = 10.42$ μm (b), 1.09 μm (c), and 0.31 μm (d) at $H = 0.3$ kOe, measured with a vibrating sample magnetometer. Here, t_{YIG} is the thickness of YIG. At $H = 1.8$ kOe (0.3 kOe), the magnetization of the YIG slab (YIG films) is aligned along the H direction. The M values for the YIG films were extracted by subtracting the contributions from the paramagnetic GGG substrates. The M data for the YIG films were detectable only for $T > 15$ K because of the large paramagnetic offset coming from the GGG substrates. The solid lines were obtained by fitting the observed M-T curves with Eq. (3).

tained the similar fitting parameters ($4.97\mu_B < M < 5.07\mu_B$ and 5.20×10^{-5} K$^{-3/2} < \zeta < 5.83 \times 10^{-5}$ K$^{-3/2}$) for all the YIG samples, indicating that the magnetic property of our YIG samples is almost the same irrespective of the YIG thickness.

In the LSSE measurements, to apply ∇T, the sample was sandwiched between two sapphire plates (1) and (2) [see Fig. 1(a)]. The sapphire (1) is thermally connected to a heat bath of which the temperature T was controlled and varied in the range from 300 K to 5 K. By applying a charge current to a chip heater attached on the top of the sapphire (2), its temperature is increased. To improve the thermal contact, thermal grease was applied between the sample and sapphire plates thinly and uniformly. The temperature difference ΔT between the sapphire (1) and (2) was measured with two thermocouples. Here, we note that the temperature gradients in the sapphire plates are negligibly small since the thermal conductivity of sapphire is much greater than that of YIG and GGG at all the temperatures [50,51]. We also note that, since the applied ΔT is much smaller than T in all the measurements [the inset to Fig. 7(a)], the LSSE can be discussed within a linear-response regime [see Figs. 1(d) and 1(e)]. We confirmed that unintended temperature differences due to thermal artifacts are negligibly small in our measurement system in all the temperature range by checking that the LSSE disappears at $\Delta T = 0$ K before each measurement. A uniform external magnetic field H was applied along the x direction by using a superconducting solenoid magnet, where the maximum H value was 90 kOe. When $H > 1$ kOe (0.15 kOe), the magnetization of the YIG slab (YIG films) is well aligned along the H direction. We also confirmed that, in the range of -90 kOe $< H <$ 90 kOe, the magnetoresistance ratio of the chip heater is $<0.03\%$ in all the temperature range and the H dependence of ΔT is negligibly small. Under this condition, we measured a dc electric voltage difference V between the ends of the Pt layer of the Pt/YIG-slab and Pt/YIG-film samples. Hereafter, to quantitatively compare the temperature dependence of the voltage signals in different samples, we mainly plot the transverse thermopower $S \equiv (V/\Delta T)(L_z/L_y)$.

III. RESULTS AND DISCUSSION

Now we start by presenting the experimental results of the LSSE in the Pt/YIG-slab sample. Figure 4(a) shows S as a function of H for various values of T, measured when H was swept between ± 90 kOe. When ∇T is applied to the sample, a clear S signal appears due to the LSSE and its sign is reversed in response to the magnetization reversal of YIG. We found that, in the Pt/YIG-slab sample, the magnitude of the S signal is suppressed by applying high magnetic fields at all the temperatures from 300 K to 5 K, while the magnitude of M at each temperature is almost constant after the saturation [compare Figs. 4(a) and 4(b)]. This suppression cannot be explained by the normal Nernst effect [52] in the Pt film since the S signal in a Pt/GGG-slab sample, in which the YIG slab is replaced with a paramagnetic GGG slab, is much smaller than the H dependence of the LSSE [see Fig. 4(a)]. The similar H dependence of the LSSE voltage was found to appear even when the thickness of the Pt layer is changed and when the Pt layer is replaced with a different metal [29], indicating that the magnetic-field-induced suppression of the LSSE in
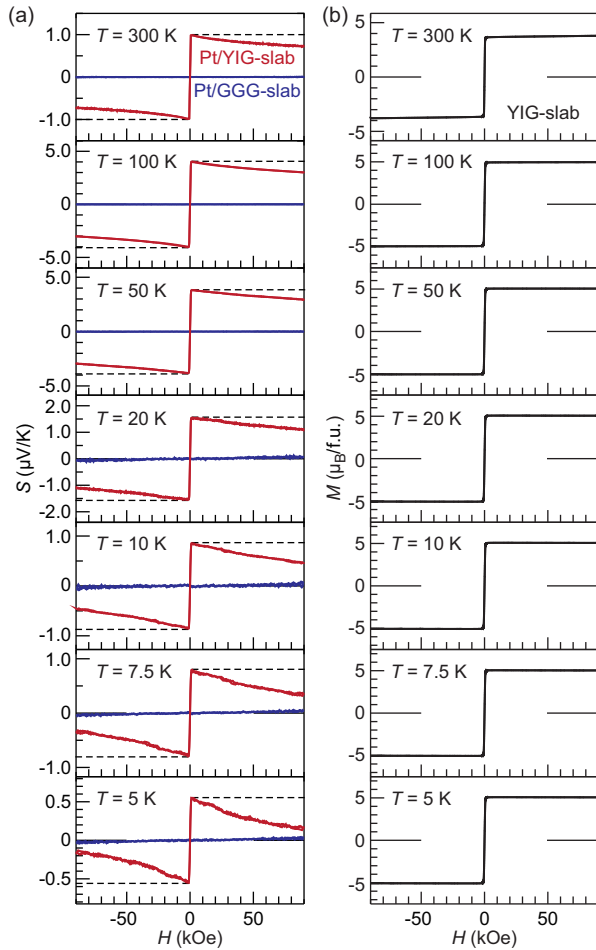
FIG. 4. (Color online) (a) H dependence of S in the Pt/YIG-slab and Pt/GGG-slab samples for various values of T, measured when H was swept between ± 90 kOe. (b) H dependence of M of the YIG slab for various values of T, measured with a vibrating sample magnetometer.

the Pt/YIG-slab sample is attributed to the YIG layer, not the paramagnetic metal layer.

In Fig. 5, we show the T dependence of S at the positive H values and of the magnetic-field-induced suppression of S in the Pt/YIG-slab sample. When the sample temperature is decreased from 300 K, the magnitude of S monotonically increases and reaches its maximum value around $T = 75$ K [see Fig. 5(a)]. On decreasing the temperature further, the S signal begins to decrease and goes to zero. This T dependence of the LSSE with peak structure is qualitatively consistent with previous results [21,31]. Importantly, as shown in Fig. 5(b), the suppression of the LSSE thermopower δ_{LSSE} also exhibits temperature dependence in the Pt/YIG-slab sample, where δ_{LSSE} is defined as $(S_{\text{max}} - S_{80\,\text{kOe}})/S_{\text{max}}$ with S_{max} and $S_{80\,\text{kOe}}$ respectively being the S values at the maximum point and at $H = 80$ kOe. We found that the suppression of the LSSE in the Pt/YIG-slab sample is almost constant ($20\% < \delta_{\text{LSSE}} < 25\%$) above 30 K and strongly enhanced below 30 K; the δ_{LSSE} value in the Pt/YIG-slab sample reaches $\sim 70\%$ at $T = 5$ K [see Fig. 5(b)].
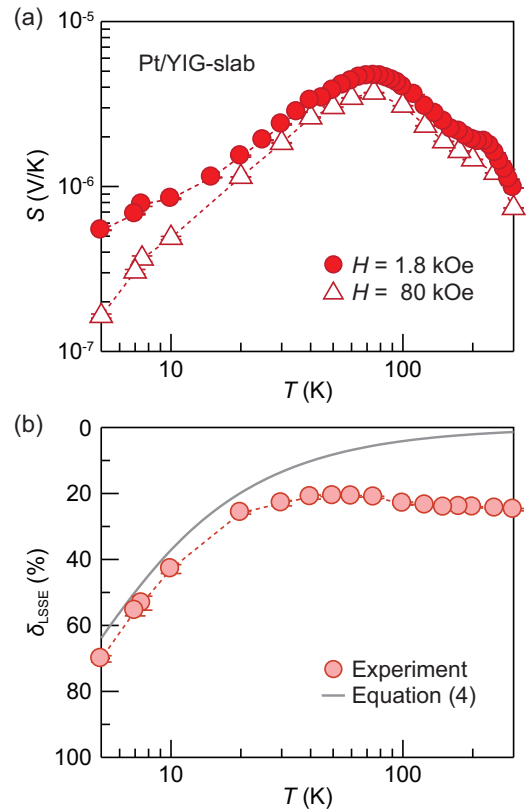

FIG. 5. (Color online) (a) Double logarithmic plot of the T dependence of S in the Pt/YIG-slab sample at $H = 1.8$ kOe (closed circles) and 80 kOe (open triangles). (b) T dependence of the suppression δ_{LSSE} of the LSSE voltage by magnetic fields in the Pt/YIG-slab sample (circles). Here, $\delta_{\text{LSSE}} \equiv (S_{\text{max}} - S_{80\,\text{kOe}})/S_{\text{max}}$ with S_{max} and $S_{80\,\text{kOe}}$ respectively being the S values at the maximum point and at $H = 80$ kOe. A gray line shows the T dependence of δ_{LSSE} calculated numerically from Eq. (4) based on the conventional formulation (see Appendix).

The critical field-induced suppression of the LSSE at low temperatures below 30 K is seemingly consistent with conventional SSE models combined with the effect of the Zeeman gap in magnon excitation. In the conventional formulation [45–47,53], the LSSE voltage V_{LSSE} is expressed as the following factor related to the magnon excitation:

$$V_{\text{LSSE}} \propto \int_{g\mu_{\text{B}}H}^{\infty} d\epsilon\, \epsilon\, \mathcal{D}(\epsilon, H)[f_{\text{BE}}(\epsilon, T_{\text{m}}) - f_{\text{BE}}(\epsilon, T_{\text{e}})]$$

$$\propto \int_{g\mu_{\text{B}}H}^{\infty} d\epsilon\, \epsilon\, \mathcal{D}(\epsilon, H) \left.\frac{\partial f_{\text{BE}}}{\partial T_{\text{m}}}\right|_{T_{\text{m}}=T}, \qquad (4)$$

where $\mathcal{D}(\epsilon, H)$ is the density of states of magnons in the ferrimagnetic insulator. To obtain the differential form in Eq. (4), we assume that the modulation of the effective temperatures induced by the external temperature gradient is very small ($T_{\text{m}} \sim T_{\text{e}}$ and $|T_{\text{m(e)}} - T| \ll T$ as demonstrated in Ref. [28]). We numerically calculated the right-hand side of Eq. (4) by assuming the density of states of parabolic exchange magnon modes: $\mathcal{D}_0\sqrt{\epsilon - g\mu_{\text{B}}H}$ with the amplitude $\mathcal{D}_0$, energy ϵ, g factor g (=2.0 for YIG), and Bohr magneton μ_{B}, where the magnon gap due to the Zeeman effect is

described as $g\mu_B H$. This parabolic dispersion well reproduces the magnon band structure of YIG in the low-energy range ($T < 30$ K) [54]. In Fig. 5(b), we compare the T dependence of δ_{LSSE} in the Pt/YIG-slab sample with that calculated from Eq. (4); below 30 K, the observed and calculated δ_{LSSE} values agree with each other within the difference of 10% (see Appendix).

The inconsistency between the observed suppression of the LSSE voltage and the conventional formulation becomes apparent with increasing the temperature. Equation (4) shows that the suppression of V_{LSSE} at $T = 300$ K is smaller than 2% even under the high magnetic fields, which is much smaller than the experimental results as shown in Fig. 5(b) ($\delta_{LSSE} \sim 25\%$ at 300 K). This is because the small Zeeman energy is defeated by thermal fluctuations when $g\mu_B H \ll k_B T$ (note that the magnon gap energy at $H = 80$ kOe corresponds to $g\mu_B H/k_B = 10.7$ K $\ll 300$ K); to affect the magnon excitation by magnetic fields, the magnon energy has to be comparable to or less than the Zeeman energy in the conventional model. In contrast, the observed large suppression of the LSSE voltage in the Pt/YIG-slab sample indicates that the magnon excitation relevant to the LSSE is affected by magnetic fields even at around room temperature, suggesting that low-frequency magnons of which the energy is comparable to the Zeeman energy (less than ~ 30 K) provide a dominant contribution to the LSSE.

The importance of low-frequency magnons in the mechanism of the LSSE is clarified by focusing on their length scale. It is notable that magnons with low frequencies exhibit long thermalization (energy relaxation) lengths [55–59], where magnons cannot be thermalized within the range less than the thermalization lengths. In the Pt/YIG systems under a temperature gradient, magnons can deviate from local thermal equilibrium, and the deviation becomes greater for magnons with longer thermalization lengths [43,55]. The frequency dependence of the magnon thermalization lengths indicates that low-frequency magnons with long thermalization lengths play a central role in the nonequilibrium states between magnons in YIG and electrons in Pt at the Pt/YIG interface. In contrast, the contribution from high-frequency magnons of which the energy is much greater than the Zeeman energy is expected to be weaker since they are closer to local thermal equilibrium due to their short thermalization lengths [56–59]. This spectral nonuniformity of the thermospin conversion can be responsible for the unexpectedly strong suppression of the LSSE voltage in the Pt/YIG-slab sample, an interpretation consistent with other fragmentary pieces of information [32,33,58,59]. Although the conventional SSE theories do not include this magnon-frequency-dependent mechanism, similar nonlocal nature has been introduced for phonon-electron systems as the concept of "spectral nonuniform temperature" in Ref. [60].

To verify the above scenario, we investigated the YIG-thickness dependence of the high-magnetic-field response of the LSSE. Because of the long-range nature of low-frequency magnons, the spectral nonuniformity of the thermospin conversion should affect the LSSE in terms of the thickness of YIG. In Fig. 6(a), we compare the H dependence of S in the Pt/YIG-slab and Pt/YIG-film samples with different YIG thicknesses ($t_{YIG} = 10.42$ μm, 1.09 μm, and 0.31 μm) at $T = 300$ K. Although we observed clear LSSE signals in
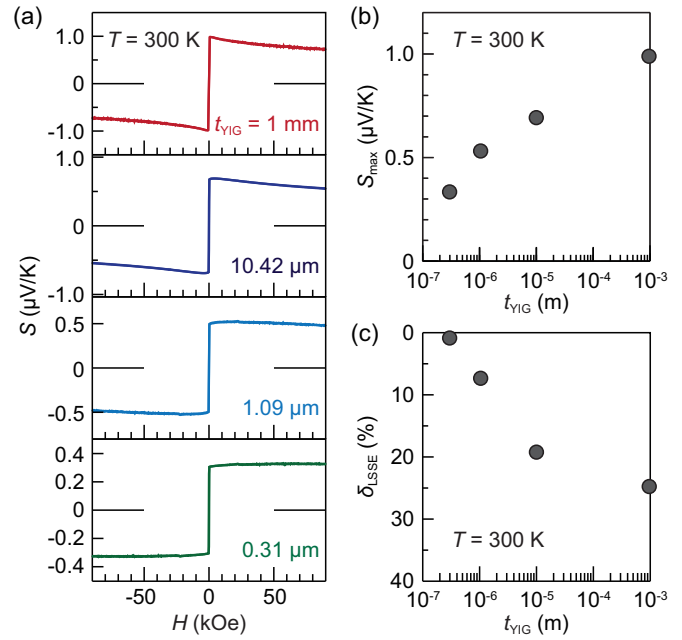

FIG. 6. (Color online) (a) H dependence of S in the Pt/YIG-slab sample with the YIG thickness of $t_{YIG} = 1$ mm and in the Pt/YIG-film samples with $t_{YIG} = 10.42$ μm, 1.09 μm, and 0.31 μm at $T = 300$ K, measured when H was swept between ± 90 kOe. (b) t_{YIG} dependence of S_{max} at $T = 300$ K. (c) t_{YIG} dependence of δ_{LSSE} at $T = 300$ K.

all the samples, the magnitude of the LSSE thermopower monotonically decreases with decreasing t_{YIG}. This behavior is consistent with the experimental results reported by Kirihara *et al.* [22] and Kehlberger *et al.* [38] [see Fig. 6(b)] [61]. This t_{YIG} dependence suggests that the magnon excitation relevant to the LSSE is limited by the boundary condition in the thin YIG films. Significantly, we found that the suppression of the LSSE by high magnetic fields, δ_{LSSE}, also monotonically decreases with decreasing t_{YIG} [Fig. 6(c)]; in the thinnest Pt/YIG-film sample with $t_{YIG} = 0.31$ μm, the LSSE signal is almost constant for $H > 0.05$ kOe ($\delta_{LSSE} \sim 1\%$ even at $H = 80$ kOe) [Fig. 6(a)]. Similar behavior was reported in Ref. [30]. This thickness dependence indicates that the contribution of low-frequency magnons, which govern the LSSE suppression in the Pt/YIG-slab sample, fades away in the Pt/YIG-film samples when the YIG thickness is less than their thermalization lengths [63]; because the long-range magnons cannot recognize the local temperature gradient in thin YIG films, such magnons are no longer in nonequilibrium. In this condition, the LSSE suppression becomes small since only remaining high-frequency magnons with the short thermalization lengths, which have energy much greater than the Zeeman energy, contribute to the LSSE.

Finally, we show the T dependence of the LSSE thermopower in the Pt/YIG-slab and Pt/YIG-film samples for various values of t_{YIG} [64]. As shown in Figs. 7(c)–7(e), in the thin Pt/YIG-film samples, no suppression of the LSSE appears even at low temperatures that satisfy the condition $g\mu_B H \sim k_B T$, which is also inconsistent with the conventional formulation described by Eq. (4) (note that, although S
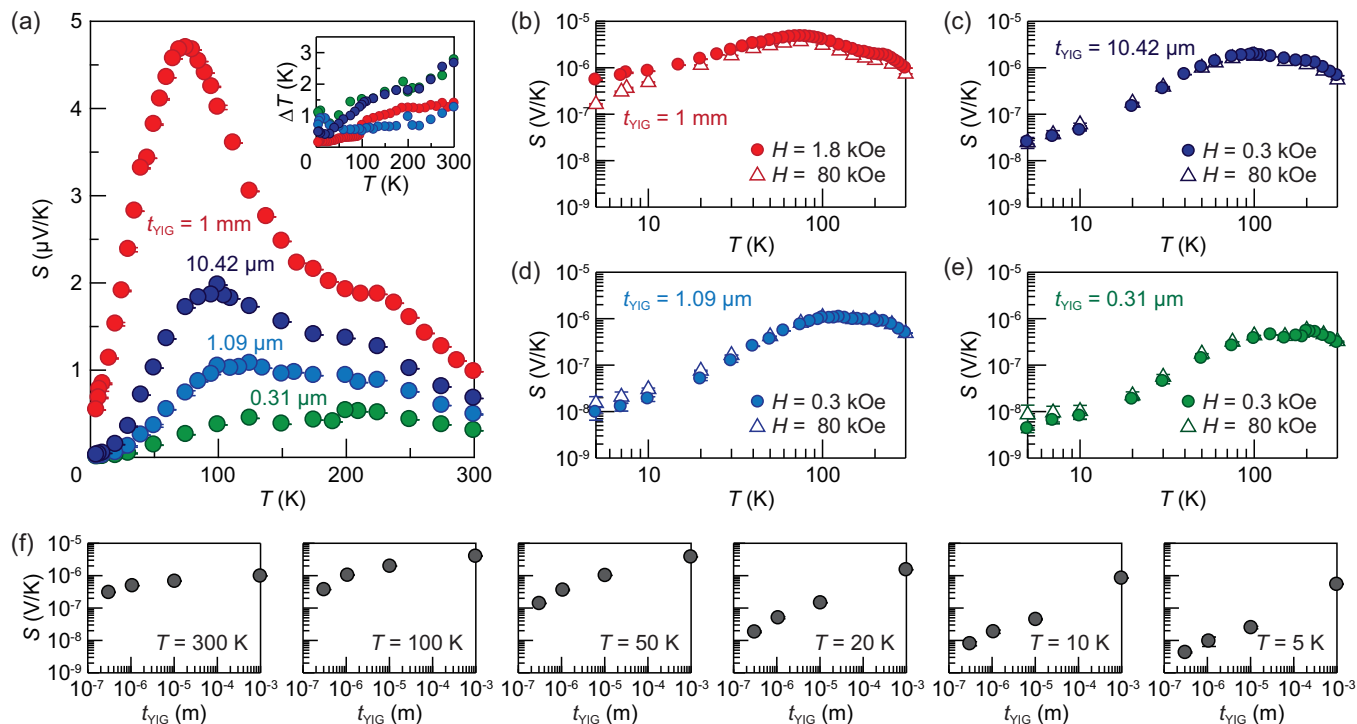
FIG. 7. (Color online) (a) T dependence of S in the Pt/YIG-slab sample at $H = 1.8$ kOe and in the Pt/YIG-film samples at $H = 0.3$ kOe. At $H = 1.8$ kOe (0.3 kOe), the magnetization of the YIG slab (YIG films) is aligned along the H direction, but the field-induced suppression of the LSSE is negligibly small. The inset to (a) shows the T dependence of ΔT applied during the LSSE measurements. (b) Comparison between the T-S curves at $H = 1.8$ kOe (closed circles) and 80 kOe (open triangles) for the Pt/YIG-slab sample with $t_{\mathrm{YIG}} = 1$ mm. (c)–(e) Comparison between the T-S curves at $H = 0.3$ kOe (closed circles) and 80 kOe (open triangles) for the Pt/YIG-film samples with $t_{\mathrm{YIG}} = 10.42\ \mu$m (c), 1.09 μm (d), and 0.31 μm (e). (f) Double logarithmic plot of the t_{YIG} dependence of S in the Pt/YIG-slab sample (Pt/YIG-film samples) at $H = 1.8$ kOe (0.3 kOe) for various values of T.

in the thin Pt/YIG film samples with $t_{\mathrm{YIG}} = 0.31$ and 1.09 μm slightly increases with increasing H at low temperatures, this behavior is attributed to the superposition of the H-linear component of the transverse thermoelectric voltage). The H dependence of the LSSE voltage in the thin Pt/YIG-film samples can be explained by the T dependence of the magnon thermalization lengths; since the thermalization length, in general, increases with decreasing T [56,57,59], the proportion of the low-frequency magnons, affected by the boundary, to the total magnon population should increase at low temperatures. This interpretation is in qualitative agreement with the t_{YIG} dependence of the LSSE; we found that the magnitude of S monotonically decreases with reducing t_{YIG} in all the temperature range [Fig. 7(a)] and the dependence on t_{YIG} of S becomes stronger at lower temperatures [Fig. 7(f)]. These results demonstrate again the importance of low-frequency magnons with long characteristic lengths in the mechanism of the LSSE.

At the end of this section, we mention a remaining task of the LSSE research. As shown in Fig. 7(a), the peak position of S shifts from low to high temperatures as t_{YIG} decreases. To understand the origin of the YIG-thickness-dependent peak shift and peak structure of the LSSE voltage, not only magnon effects [31,54] but also phonon effects [46,59] should be taken into account in the mechanism of the LSSE; the separation and quantitative evaluation of these contributions are necessary. An indispensable requirement for obtaining the complete

understanding of the temperature dependence of the LSSE is the precise determination of the temperature-gradient distribution in YIG-film/GGG-substrate systems, which enables the quantitative investigation of the YIG-thickness dependence of the LSSE. A challenge for the quantitative evaluation of the temperature distribution in LSSE devices is already in progress [65].

IV. CONCLUSION

In this study, we have investigated temperature and thickness dependencies of high-magnetic-field response of the longitudinal spin Seebeck effect (LSSE) in Pt/$Y_3Fe_5O_{12}$ (YIG) junction systems. The experimental results show that the LSSE signal is suppressed by applying high magnetic fields at the temperatures ranging from 300 K to 5 K and this suppression is enhanced with decreasing the temperature in the Pt/YIG-slab system. The suppression of the LSSE appears even when the magnon gap induced by the Zeeman effect $g\mu_{\mathrm{B}}H$ is much less than the thermal energy $k_{\mathrm{B}}T$, suggesting that low-frequency magnons with energy comparable to or less than the Zeeman energy provide a dominant contribution to the LSSE rather than the higher-frequency magnons. This spectral nonuniformity of the thermospin conversion is associated with the characteristic lengths of the LSSE since the LSSE signal and its magnetic field dependence are strongly affected by the thickness of YIG. We anticipate that the comprehensive LSSE

data reported here fill in the missing piece of the mechanism of the LSSE and lead to the development of theories of spin-current physics.

Note added. Recently, Jin *et al.* [66], Ritzmann *et al.* [67], and Guo *et al.* [62] also reported the high-magnetic-field dependence of the LSSE in Pt/YIG systems. The experimental results and basic interpretation of these studies are consistent with those of the present study.

APPENDIX: NUMERICAL CALCULATION OF EQ. (4)

To clarify the H dependence of the LSSE voltage V_{LSSE} described by the conventional formulation, we numerically calculated the right-hand side of Eq. (4). For simplicity, we assume that magnons have a parabolic dispersion relation, where the density of states of magnons is affected by the Zeeman energy [68]. As shown in Fig. 8(a), the magnon gap opening due to the Zeeman effect is much smaller than thermal energy near room temperature even when the high magnetic field of $H = 80$ kOe is applied. Figure 8(b) shows
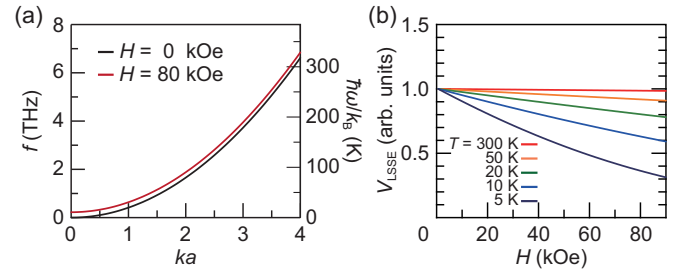

FIG. 8. (Color online) (a) Parabolic dispersion relations of magnons at $H = 0$ kOe and 80 kOe in units of the magnon frequency f ($=\omega/2\pi$) and corresponding temperature $\hbar\omega/k_{\mathrm{B}}$. The parabolic magnon dispersion includes the Zeeman gap: $\hbar\omega = Da^2k^2 + g\mu_{\mathrm{B}}H$, where ω is the angular frequency, k is the magnon wave number, a is the lattice constant of YIG ($=12.376$ Å) [49], and D is the spin-wave stiffness constant. Here, we use $Da^2 = 4.2 \times 10^{-29}$ erg cm^2 [54,69]. (b) H dependence of V_{LSSE} for various values of T, calculated from Eq. (4).

the calculation results of the H dependence of V_{LSSE} for various values of T. We found that, although V_{LSSE} described by Eq. (4) is suppressed by magnetic fields at low temperatures, the suppression around room temperature is much smaller than the observed H dependence of the LSSE for the Pt/YIG-slab sample [compare Figs. 4(a) and 8(b)]. In Fig. 5(b), we plot the T dependence of δ_{LSSE} calculated from Eq. (4), which is defined as $(V_{\mathrm{LSSE}}^{\max} - V_{\mathrm{LSSE}}^{80\mathrm{kOe}})/V_{\mathrm{LSSE}}^{\max}$ with $V_{\mathrm{LSSE}}^{\max}$ and $V_{\mathrm{LSSE}}^{80\mathrm{kOe}}$ respectively being the V_{LSSE} values at the maximum point and at $H = 80$ kOe, indicating that the inconsistency between the experimental results and Eq. (4) increases with increasing T. As discussed above, the small suppression of V_{LSSE} is attributed to the large energy difference between $g\mu_{\mathrm{B}}H$ and $k_{\mathrm{B}}T$, showing the importance of low-frequency magnons in the mechanism of the LSSE. Finally, we note that the integrand of Eq. (4) consists of $\epsilon\mathcal{D}f_{\mathrm{BE}}$, while that of the magnon number is $\mathcal{D}f_{\mathrm{BE}}$ alone; since the factor ϵ in the integrand of Eq. (4) eliminates the singularity of f_{BE} at $\epsilon = 0$, the calculated values do not reach $V_{\mathrm{LSSE}} = 0$ even when $g\mu_{\mathrm{B}}H > k_{\mathrm{B}}T$ [see Fig. 8(b)].

[1] A. G. Gurevich and G. A. Melkov, *Magnetization Oscillations and Waves* (CRC, Boca Raton, FL, 1996).

[2] V. Cherepanov, I. Kolokolov, and V. L'vov, The saga of YIG: Spectra, thermodynamics, interaction, and relaxation of magnons in a complex magnet, Phys. Rep. **229**, 81 (1993).

[3] G. P. Rodrigue, H. Meyer, and R. V. Jones, Resonance measurements in magnetic garnets, J. Appl. Phys. **31**, S376 (1960).

[4] I. S. Tupitsyn, P. C. E. Stamp, and A. L. Burin, Stability of Bose-Einstein condensates of hot magnons in yttrium iron garnet films, Phys. Rev. Lett. **100**, 257202 (2008).

[5] G. E. W. Bauer, E. Saitoh, and B. J. van Wees, Spin caloritronics, Nat. Mater. **11**, 391 (2012).

[6] S. R. Boona, R. C. Myers, and J. P. Heremans, Spin caloritronics, Energy Environ. Sci. **7**, 885 (2014).

[7] S. Maekawa, H. Adachi, K. Uchida, J. Ieda, and E. Saitoh, Spin current: Experimental and theoretical aspects, J. Phys. Soc. Jpn. **82**, 102002 (2013).

[8] Y. Kajiwara, K. Harii, S. Takahashi, J. Ohe, K. Uchida, M. Mizuguchi, H. Umezawa, H. Kawai, K. Ando, K. Takanashi, S. Maekawa, and E. Saitoh, Transmission of electrical signals by spin-wave interconversion in a magnetic insulator, Nature (London) **464**, 262 (2010).

[9] Y. Tserkovnyak, A. Brataas, G. E. W. Bauer, and B. I. Halperin, Nonlocal magnetization dynamics in ferromagnetic heterostructures, Rev. Mod. Phys. **77**, 1375 (2005).

[10] M. Weiler, M. Althammer, M. Schreier, J. Lotze, M. Pernpeintner, S. Meyer, H. Huebl, R. Gross, A. Kamra, J. Xiao, Y.-T. Chen, H. Jiao, G. E. W. Bauer, and S. T. B. Goennenwein, Experimental test of the spin mixing

interface conductivity concept, Phys. Rev. Lett. **111**, 176601 (2013).

[11] Z. Qiu, K. Ando, K. Uchida, Y. Kajiwara, R. Takahashi, H. Nakayama, T. An, Y. Fujikawa, and E. Saitoh, Spin mixing conductance at a well-controlled platinum/yttrium iron garnet interface, Appl. Phys. Lett. **103**, 092404 (2013).

[12] A. Azevedo, L. H. Vilela-Leão, R. L. Rodríguez-Suárez, A. B. Oliveira, and S. M. Rezende, dc effect in ferromagnetic resonance: Evidence of the spin-pumping effect?, J. Appl. Phys. **97**, 10C715 (2005).

[13] E. Saitoh, M. Ueda, H. Miyajima, and G. Tatara, Conversion of spin current into charge current at room temperature: Inverse spin-Hall effect, Appl. Phys. Lett. **88**, 182509 (2006).

[14] K. Uchida, S. Takahashi, K. Harii, J. Ieda, W. Koshibae, K. Ando, S. Maekawa, and E. Saitoh, Observation of the spin Seebeck effect, Nature (London) **455**, 778 (2008).

[15] K. Uchida, J. Xiao, H. Adachi, J. Ohe, S. Takahashi, J. Ieda, T. Ota, Y. Kajiwara, H. Umezawa, H. Kawai, G. E. W. Bauer, S. Maekawa, and E. Saitoh, Spin Seebeck insulator, Nat. Mater. **9**, 894 (2010).

[16] C. M. Jaworski, J. Yang, S. Mack, D. D. Awschalom, J. P. Heremans, and R. C. Myers, Observation of the spin-Seebeck effect in a ferromagnetic semiconductor, Nat. Mater. **9**, 898 (2010).

[17] K. Uchida, H. Adachi, T. Ota, H. Nakayama, S. Maekawa, and E. Saitoh, Observation of longitudinal spin-Seebeck effect in magnetic insulators, Appl. Phys. Lett. **97**, 172505 (2010).

[18] C. M. Jaworski, J. Yang, S. Mack, D. D. Awschalom, R. C. Myers, and J. P. Heremans, Spin-Seebeck effect: A phonon driven spin distribution, Phys. Rev. Lett. **106**, 186601 (2011).

[19] K. Uchida, H. Adachi, T. An, T. Ota, M. Toda, B. Hillebrands, S. Maekawa, and E. Saitoh, Long-range spin Seebeck effect and acoustic spin pumping, Nat. Mater. **10**, 737 (2011).

[20] M. Weiler, M. Althammer, F. D. Czeschka, H. Huebl, M. S. Wagner, M. Opel, I.-M. Imort, G. Reiss, A. Thomas, R. Gross, and S. T. B. Goennenwein, Local charge and spin currents in magnetothermal landscapes, Phys. Rev. Lett. **108**, 106602 (2012).

[21] K. Uchida, T. Ota, H. Adachi, J. Xiao, T. Nonaka, Y. Kajiwara, G. E. W. Bauer, S. Maekawa, and E. Saitoh, Thermal spin pumping and magnon-phonon-mediated spin-Seebeck effect, J. Appl. Phys. **111**, 103903 (2012).

[22] A. Kirihara, K. Uchida, Y. Kajiwara, M. Ishida, Y. Nakamura, T. Manako, E. Saitoh, and S. Yorozu, Spin-current-driven thermoelectric coating, Nat. Mater. **11**, 686 (2012).

[23] D. Qu, S. Y. Huang, J. Hu, R. Wu, and C. L. Chien, Intrinsic spin Seebeck effect in Au/YIG, Phys. Rev. Lett. **110**, 067206 (2013).

[24] T. Kikkawa, K. Uchida, Y. Shiomi, Z. Qiu, D. Hou, D. Tian, H. Nakayama, X.-F. Jin, and E. Saitoh, Longitudinal spin Seebeck effect free from the proximity Nernst effect, Phys. Rev. Lett. **110**, 067207 (2013).

[25] D. Meier, T. Kuschel, L. Shen, A. Gupta, T. Kikkawa, K. Uchida, E. Saitoh, J.-M. Schmalhorst, and G. Reiss, Thermally driven spin and charge currents in thin NiFe$_2$O$_4$/Pt films, Phys. Rev. B **87**, 054421 (2013).

[26] R. Ramos, T. Kikkawa, K. Uchida, H. Adachi, I. Lucas, M. H. Aguirre, P. Algarabel, L. Morellón, S. Maekawa, E. Saitoh, and M. R. Ibarra, Observation of the spin Seebeck effect in epitaxial Fe$_3$O$_4$ thin films, Appl. Phys. Lett. **102**, 072413 (2013).

[27] K. Uchida, T. Nonaka, T. Kikkawa, Y. Kajiwara, and E. Saitoh, Longitudinal spin Seebeck effect in various garnet ferrites, Phys. Rev. B **87**, 104412 (2013).

[28] M. Schreier, A. Kamra, M. Weiler, J. Xiao, G. E. W. Bauer, R. Gross, and S. T. B. Goennenwein, Magnon, phonon, and electron temperature profiles and the spin Seebeck effect in magnetic insulator/normal metal hybrid structures, Phys. Rev. B **88**, 094410 (2013).

[29] T. Kikkawa, K. Uchida, S. Daimon, Y. Shiomi, H. Adachi, Z. Qiu, D. Hou, X.-F. Jin, S. Maekawa, and E. Saitoh, Separation of longitudinal spin Seebeck effect from anomalous Nernst effect: Determination of origin of transverse thermoelectric voltage in metal/insulator junctions, Phys. Rev. B **88**, 214403 (2013).

[30] M. Schreier, N. Roschewsky, E. Dobler, S. Meyer, H. Huebl, R. Gross, and S. T. B. Goennenwein, Current heating induced spin Seebeck effect, Appl. Phys. Lett. **103**, 242404 (2013).

[31] S. M. Rezende, R. L. Rodríguez-Suárez, R. O. Cunha, A. R. Rodrigues, F. L. A. Machado, G. A. Fonseca Guerra, J. C. Lopez Ortiz, and A. Azevedo, Magnon spin-current theory for the longitudinal spin-Seebeck effect, Phys. Rev. B **89**, 014416 (2014).

[32] N. Roschewsky, M. Schreier, A. Kamra, F. Schade, K. Ganzhorn, S. Meyer, H. Huebl, S. Geprägs, R. Gross, and S. T. B. Goennenwein, Time resolved spin Seebeck effect experiments, Appl. Phys. Lett. **104**, 202410 (2014).

[33] M. Agrawal, V. I. Vasyuchka, A. A. Serga, A. Kirihara, P. Pirro, T. Langner, M. B. Jungfleisch, A. V. Chumak, E. Th. Papaioannou, and B. Hillebrands, Role of bulk-magnon transport in the temporal evolution of the longitudinal spin-Seebeck effect, Phys. Rev. B **89**, 224414 (2014).

[34] K. Uchida, M. Ishida, T. Kikkawa, A. Kirihara, T. Murakami, and E. Saitoh, Longitudinal spin Seebeck effect: From fundamentals to applications, J. Phys.: Condens. Matter **26**, 343202 (2014).

[35] A. Aqeel, I. J. Vera-Marun, B. J. van Wees, and T. T. M. Palstra, Surface sensitivity of the spin Seebeck effect, J. Appl. Phys. **116**, 153705 (2014).

[36] K. Uchida, T. Kikkawa, A. Miura, J. Shiomi, and E. Saitoh, Quantitative temperature dependence of longitudinal spin Seebeck effect at high temperatures, Phys. Rev. X **4**, 041023 (2014).

[37] M. Schreier, G. E. W. Bauer, V. I. Vasyuchka, J. Flipse, K. Uchida, J. Lotze, V. Lauer, A. V. Chumak, A. A. Serga, S. Daimon, T. Kikkawa, E. Saitoh, B. J. van Wees, B. Hillebrands, R. Gross, and S. T. B. Goennenwein, Sign of inverse spin Hall voltages generated by ferromagnetic resonance and temperature gradients in yttrium iron garnet platinum bilayers, J. Phys. D: Appl. Phys. **48**, 025001 (2015).

[38] A. Kehlberger, R. Röser, G. Jakob, U. Ritzmann, D. Hinzke, U. Nowak, M. C. Onbasli, D. H. Kim, C. A. Ross, M. B. Jungfleisch, B. Hillebrands, and M. Kläui, Determination of the origin of the spin Seebeck effect—bulk vs interface effects, arXiv:1306.0784.

[39] J. Flipse, F. K. Dejene, D. Wagenaar, G. E. W. Bauer, J. Ben Youssef, and B. J. van Wees, Observation of the spin Peltier effect for magnetic insulators, Phys. Rev. Lett. **113**, 027601 (2014).

[40] S. O. Valenzuela and M. Tinkham, Direct electronic measurement of the spin Hall effect, Nature (London) **442**, 176 (2006).

[41] M. V. Costache, M. Sladkov, S. M. Watts, C. H. van der Wal, and B. J. van Wees, Electrical detection of spin pumping due to the precessing magnetization of a single ferromagnet, Phys. Rev. Lett. **97**, 216603 (2006).

[42] T. Kimura, Y. Otani, T. Sato, S. Takahashi, and S. Maekawa, Room-temperature reversible spin Hall effect, Phys. Rev. Lett. **98**, 156601 (2007).

[43] J. Xiao, G. E. W. Bauer, K. Uchida, E. Saitoh, and S. Maekawa, Theory of magnon-driven spin Seebeck effect, Phys. Rev. B **81**, 214418 (2010).

[44] H. Adachi, K. Uchida, E. Saitoh, J. Ohe, S. Takahashi, and S. Maekawa, Gigantic enhancement of spin Seebeck effect by phonon drag, Appl. Phys. Lett. **97**, 252506 (2010).

[45] H. Adachi, J. Ohe, S. Takahashi, and S. Maekawa, Linear-response theory of spin Seebeck effect in ferromagnetic insulators, Phys. Rev. B **83**, 094410 (2011).

[46] H. Adachi, K. Uchida, E. Saitoh, and S. Maekawa, Theory of the spin Seebeck effect, Rep. Prog. Phys. **76**, 036501 (2013).

[47] S. Hoffman, K. Sato, and Y. Tserkovnyak, Landau-Lifshitz theory of the longitudinal spin Seebeck effect, Phys. Rev. B **88**, 064408 (2013).

[48] S. Y. Huang, X. Fan, D. Qu, Y. P. Chen, W. G. Wang, J. Wu, T. Y. Chen, J. Q. Xiao, and C. L. Chien, Transport magnetic proximity effects in platinum, Phys. Rev. Lett. **109**, 107204 (2012).

[49] M. A. Gilleo and S. Geller, Magnetic and crystallographic properties of substituted yttrium-iron garnet, $3Y_2O_3 \cdot xM_2O_3 \cdot (5-x)Fe_2O_3$, Phys. Rev. **110**, 73 (1958).

[50] G. A. Slack, Thermal conductivity of MgO, Al_2O_3, $MgAl_2O_4$, and Fe_3O_4 crystals from $3°$ to $300°$ K, Phys. Rev. **126**, 427 (1962).

[51] G. A. Slack and D. W. Oliver, Thermal conductivity of garnets and phonon scattering by rare-earth ions, Phys. Rev. B **4**, 592 (1971).

[52] W. Nernst, Ueber die electromotorischen Kräfte, welche durch den Magnetismus in von einem Wärmestrome durchflossenen Metallplatten geweckt werden, Ann. Phys. (Leipzig) **267**, 760 (1887).

[53] S. A. Bender, R. A. Duine, and Y. Tserkovnyak, Electronic pumping of quasiequilibrium Bose-Einstein-condensed magnons, Phys. Rev. Lett. **108**, 246601 (2012).

[54] J. S. Plant, "Pseudo-acoustic" magnon dispersion in yttrium iron garnet, J. Phys. C **16**, 7037 (1983).

[55] D. J. Sanders and D. Walton, Effect of magnon-phonon thermal relaxation on heat transport by magnons, Phys. Rev. B **15**, 1489 (1977).

[56] S. S.-L. Zhang and S. Zhang, Magnon mediated electric current drag across a ferromagnetic insulator layer, Phys. Rev. Lett. **109**, 096603 (2012).

[57] S. S.-L. Zhang and S. Zhang, Spin convertance at magnetic interfaces, Phys. Rev. B **86**, 214424 (2012).

[58] M. Agrawal, V. I. Vasyuchka, A. A. Serga, A. D. Karenowska, G. A. Melkov, and B. Hillebrands, Direct measurement of magnon temperature: New insight into magnon-phonon coupling in magnetic insulators, Phys. Rev. Lett. **111**, 107204 (2013).

[59] S. R. Boona and J. P. Heremans, Magnon thermal mean free path in yttrium iron garnet, Phys. Rev. B **90**, 064421 (2014).

[60] K. S. Tikhonov, J. Sinova, and A. M. Finkel'stein, Spectral non-uniform temperature and non-local heat transfer in the spin Seebeck effect, Nat. Commun. **4**, 1945 (2013).

[61] According to Refs. [38] and [62], we can fit the thickness dependence of the magnitude of the LSSE voltage in Fig. 6(b) with $\mathcal{S}[1 - \exp(-t_{YIG}/\xi)]$, where $\mathcal{S}$ and ξ are adjustable parameters. ξ was estimated to be ~ 1 μm, which is consistent with the value reported in Ref. [62].

[62] E.-J. Guo, A. Kehlberger, J. Cramer, G. Jakob, and M. Kläui, Origin of the thickness-dependent low-temperature enhancement of spin Seebeck effect in YIG films, arXiv:1506.06037.

[63] Our result indicates that the characteristic length of the LSSE for low-frequency magnons, affected by the Zeeman energy in $|H| < 90$ kOe, is at least greater than 0.31 μm at room temperature. However, to discuss the characteristic length associated with the LSSE suppression and its magnon-frequency dependence quantitatively, one has to determine the spectral nonuniformity of the thermospin conversion. Unfortunately, it is difficult to make this quantitative evaluation at the present stage.

[64] We note that, in the Pt/YIG-film samples at low temperatures, the temperature-gradient distribution in the thickness direction may be affected by the difference in the thermal conductivity between YIG and GGG, since the temperature dependence of the thermal conductivity of YIG is different from that of GGG and the thermal conductivity of YIG may depend on the YIG thickness at low temperatures [65], a situation which makes it difficult to evaluate the temperature difference between the top and bottom of the YIG films and the absolute magnitude of the LSSE voltage quantitatively. Nevertheless, even in this situation, we can discuss the field-induced suppression of the LSSE voltage in the Pt/YIG-film samples quantitatively, since it is defined as the relative ratio between the LSSE voltages at low and high magnetic fields.

[65] C. Euler, P. Hołuj, T. Langner, A. Kehlberger, V. I. Vasyuchka, M. Kläui, and G. Jakob, Thermal conductance of thin film YIG determined using Bayesian statistics, arXiv:1505.08006.

[66] H. Jin, S. R. Boona, Z. Yang, R. C. Myers, and J. P. Heremans, The effect of the magnon dispersion on the longitudinal spin Seebeck effect in yttrium iron garnets (YIG), arXiv:1504.00895.

[67] U. Ritzmann, D. Hinzke, A. Kehlberger, E.-J. Guo, M. Kläui, and U. Nowak, Magnetic field control of the spin Seebeck effect, arXiv:1506.05290.

[68] C. Kittel, *Quantum Theory of Solids*, 2nd revised printing (John Wiley and Sons, New York, 1987).

[69] C. M. Srivastava and R. Aiyar, Spin wave stiffness constants in some ferrimagnetics, J. Phys. C **20**, 1119 (1987).